Abundances in the Planetary Nebula IC 5217

Siek Hyung[1], Lawrence H. Aller[2], Walter A. Feibelman[3], Woo-Baik Lee[1]

[1]*Korea Astronomy Observatory, 61-1 Whaam-dong, Yusong-gu, Taejon 305-348, Korea*
[2]*Physics and Astronomy Department, University of California, Los Angeles, California 90095*
[3]*Laboratory for Astronomy and Solar Physics, Code 684.1, NASA Goddard Space Flight Center, Greenbelt, MD 20771*

ABSTRACT

High resolution optical wavelength spectroscopic data were secured in the optical wavelengths, 3700Å – 10 050Å, for the planetary nebula IC 5217 with the Hamilton Echelle Spectrograph at Lick Observatory. These optical spectra have been analyzed along with the near-UV and UV archive data. Diagnostic analyses indicate a nebular physical condition with electron temperature of about 10 700 K (from the [O III] lines) and the density of $N_\epsilon = 5000$ cm^{-1}. Ionic concentrations have been derived with the representative diagnostics, and with the aid of a photoionization model construction, we derived the elemental abundances. Contrary to the previous studies found in the literature, He and C appear to be depleted compared to the average planetary nebula and to the Sun (and S marginally so), while the remaining elements appear to be close to the average value. IC 5217 may have evolved from an O-rich progenitor and the central star temperature of IC 5217 is likely to be 92 000 K.

Subject headings: ISM: planetary nebulae: abundance: plasma diagnostics: individual (IC 5217)

1. Introduction

IC 5217 is an elongated planetary nebula (PN) with an equator/pole contrast (e/p) ratio exceeding 4. In a butterfly PN, as distinct from an elliptical one, the equator/pole density contrast commonly described by the parameter, e/p, is ~2 for ordinary ellipticals and it can reach a factor as high as 15 for extreme butterfly structures. The elongation may be caused by a rapid spherical wind driven by the central star of the planetary nebula (CSPN) which is rapidly evolving into a white dwarf. Icke et al. (1987) interpret IC 5217 as an 'early butterfly' with a sharp ionization front only in selected parts of its boundary, which resembles the Red Rectangle, showing evidence of bipolar shocks. In the [N II] line profile, the bright inner region appears to have kinematics of a ring, or perhaps a disk with a central hole, expanding at 25 km s^{-1} and seen nearly edge on (see

Balick 1987). The expansion velocities may have a positional variation, i.e. ~16 km s^{-1} ([O III]) and 25–28 km s^{-1} ([N II]).

The medium excitation of IC 5217 (excitation class 6: Aller & Liller 1968) with the numerous lines in its spectrum, and its elongated structure, offers the possibility of obtaining improved plasma diagnostics and abundances. The spectrum was first described in the classic investigation by Wyse (1942). Later, Aller and Czyzak (1979, hereafter AC79) carried out relatively detailed studies with the image tube scanner (ITS), but there are not many secured spectral lines, and the observed lines are of a relatively very poor wavelength dispersion in the early pioneering works. The advent of charge coupled devices (CCDs) and the echelle spectrograph has made it possible to take advantage of high spectral resolution and accuracy. We obtained a high dispersion optical spectrum from 3700 to 10 050Å with Hamilton Echelle Spectrograph (HES, hereafter) at Lick Observatory.

Our objective is not only to obtain a reliable spectrum in the optical wavelengths, but also to investigate the diagnostics and abundances based on a fuller coverage of spectrum. Thus, we will analyze the spectrum of the HES along with those of the near UV region secured by Likkel and Aller (1986, hereafter LA86) with an image tube scanner and International Ultraviolet Explorer (*IUE*) Archive data in the UV region. First, we describe the *IUE*, near-UV ITS spectra and HES observations, and then we present the line identifications for the data sets. Based on the ions observed, we will obtain the diagnostics from which we will compute the ionic concentrations. We then construct a photoionization model which can represent most of the observed line intensities, and as a result determine the abundances. Finally, we compare the chemical abundance of IC 5217 with the solar and average nebular abundance, and discuss briefly its evolutionary status. Table 1 gives some basic data for IC 5217 and useful references.

2. Observations

All the *IUE* spectra are low dispersion, except for SWP 08175, and they were taken through the large (10″ × 23″ oval) entrance aperture of the *IUE* cameras. A line-by-line echelle analysis indicates that the object was centered in the aperture. The archival data, processed by the NEWSIPS routine, were reduced with the latest *IUE* reduction techniques at Goddard Space Fight Center (GPFC).

The angular apparent sizes of IC 5217 are small enough to fit into the large entrance aperture so that all the nebular flux was intercepted. Table 2 gives the log of the *IUE* observations of IC 5217. In Fig. 1, we plot the combined *IUE* SWP and LWR spectra in the wavelengths from 1200 to 3250 Å (an extinction correction was applied with E(B-V) = 0.39). All spectra were smoothed with a 3-point average. We measured the spectrum from the three coadded SWP spectra (SWP 01923, 06257, 41909) and one LWR archive (LWR 05429), and we ignored the others. Our new measurements are given in Table 3. Successive columns of Table 3 give the observed and laboratory wavelengths, the ion, Seaton's extinction parameter, k_λ, the extinction corrected intensity with E(B-V) = 0.39 [relative to I(Hβ) = 100], and the measured flux in units of 10^{-13} ergs cm^{-2} s^{-1}.

For the near UV region (from the limit of the Balmer series down to the atmospheric cutoff near 3000Å), we rely primarily on the LA86 observations obtained with the Lick 3-m telescope, using a 'green' tube of high sensitivity. They investigated the Bowen fluorescent mechanism of the O III lines. In this region fall lines of He I, He II, O II, O IV, [Ne III] (auroral-type), [Ne V], and [Na IV]. Note that the entrance slot has a length of 4″ and a width of 2″ and the spectral resolution is about 4Å. The Hamilton echelle observations were secured with a slit width of 640 μm (~1.2″) and a slit length of 4″. The spectral purity of the ITS is therefore inferior to that of the 3-m Coude Hamilton Echelle Spectrograph. Table 4 gives the near UV measurements by Likkel (LA86). The first column gives the measured wavelength due to LA86; the second column gives the laboratory identification; the extinction parameter, k_λ, is listed in column (3). Column (4) gives the derived intensity corrected for interstellar extinction with $C = 0.34$; column (5) gives the measured flux data secured by LA86 from the green tube ITS observations. Here, flux and intensity are both given on the scale of I(Hβ) = 100 ($C = 0.54$) and F(Hβ) = 100. 'B' in the last column denotes Bowen O III lines, which have been reviewed by LA86.

Table 5 gives the log of the Hamilton observations. The optical region observations were all obtained with the Hamilton Echelle Spectrograph (HES) at the coude focus of the 3 m Shane telescope of Lick Observatory, in 1991 September/October, 1995 July, and 1997 August. We used a small CCD chip of 800×800 pixels in 1991. Since this CCD chip could not cover the entire optical wavelength range, several chip set-ups were required in 1991 observation (see Table 5): set-up 121 for all the lines shortward of 4300Å; set-ups 123 and 127 for the region 4200 ~ 6700Å, and set-up 125 for wavelengths larger than 6000Å. However, we need 3 more chip settings to cover the whole echelle pattern for the entire optical wavelength region. See Hyung (1994) for an explanation of additional chip settings. Although we did not cover the full echelle pattern with this small CCD chip, two larger 2048×2048 pixel CCDs which were available later, could cover the whole HES echelle pattern. The 800 pixel CCD in 1991 and 2048 pixel CCDs in 1997 were more efficient than that the one in 1995. For each chip setting, we obtained exposures of the Th-Ar arc to set wavelengths, and a dome-quartz lamp to fix a flat field, i.e., allowing for correction of pixel to pixel sensitivity fluctuations, and of comparison stars of known energy distribution, e.g. BD+284211 and 58 Aql. The reduction procedures are described by Hyung (1994).

We summarized the HES results in Table 6. A large number of optical lines are measured. Successive columns give the measured wavelength (corrected for radial velocity), the wavelength of the most probable identification, the ion, multiplet number from Ms Moore's tabulations (1974, 1993), and Seaton's extinction parameter, k_λ. We found the radial velocity of IC 5217 to be -101.42 ± 0.38 km·s^{-1}, while Acker et al. (1992) quote -98.6 ± 0.4 km·s^{-1}. The 6th column gives the intensity on the scale I(4861) = 100.0 corrected for interstellar extinction with an extinction coefficient $C = \log$ I(Hβ)/F(β) = 0.7, found from Balmer line ratios such as $F(H\alpha)/F(H\beta)$, and from a comparison of Balmer and Paschen lines; this value is higher than those found by other observers or that of the *IUE* region, e.g., C=0.45 (AC79). In fact, our estimation of the extinction coefficient for the HES data is probably an overestimation caused by an improper response function.

The 7th column presents the flux on the scale of F(4861) = 100.0, while the last column lists the formal root mean square (RMS) % error as deduced from internal disagreement of measurements made with different chip settings (when two or more independent measurements are available). We employed the same extinction coefficients for the UV and near UV spectral lines, but used different value for the optical wavelength. This different choice of C in the optical region seems inevitable, due to the response functions involved. In Table 6 and in the following Tables, we have given more significant figures than the data justify, to avoid rounding off errors.

3. Ionic Concentrations

3.1. Overview of Diagnostics

Numerous lines, including many strategically important ones, especially useful for nebular diagnostic and abundance determinations, are observed in the optical spectrum of of IC 5217. Note also the richness of the *IUE* ionic spectra in this PN. The following ions are detected in the spectrum of IC 5217: H, He I, He II, C I?, C II, C II], C III, C III], C IV, N II, [N II], N III, N III], [O I], O II, [O II], O III, O III], [O III], O IV, O V?, O V] (P Cyg)?, Ne II, [Ne III], [Ne IV], [Ne V]?, Si II, Si III], [S II], [S III], [Cl III], [Cl IV], Ar II, [Ar III], [Ar IV], [Ar V], [K IV], Na IV, [Mn V]?, Fe I?, [Fe III], and [Fe VII]. The UV lines are the following: He I, He II, C I?, C II], C III], C IV, N III, N IV], N V, O I, [O II], O III, O III], O IV], [Ne III], [Ne IV], [Ne V], [Mg V], Si III], Si IV, and [Ar IV]. Diagnostic line ratios suitable for fixing (N_ϵ,T_ϵ) are listed in Table 7.

Fig. 2 shows the diagnostic diagram. Data of electronic collision strengths involving the plasma and nebular diagnostics were constantly updated in our previous investigations, e.g. Hyung and Aller (1996). With the Kastner & Bhatia (1984) classification method, i.e. N III 1750/4640 ratio as a discriminant of excitation. An HES line ratio of 12.66 gives the excitation class of 9. However, the N III 1750/4640 ratio applies only to CSPN. In a PN of excitation 9, [Ne IV] and [Ne V] would be very prominent, but the evidence for [Ne V] is very unconvincing: λ1575 is weak. The best and the most reliable one would be the He II4686/Hβ ratio ~ 0.1, which gives excitation class 6 (see Fig. 1 of Aller & Liller 1968). The diagnostics indicate relatively higher electron temperatures, in spite of an intermediate excitation nebula: from the [O III] [4959+5007]/4363 ratio, we get T_ϵ of about 10 700 K, while [Ar III] gives $T_\epsilon \sim$ 11 700 K. For the lower excitation line ratios, we find a similar electron temperature, i.e. T_ϵ([N II]) ~ 11 000 K. For high excitation ions, it is probably higher than the above. We find T_ϵ([Cl IV]) ~ 16 000 K, which is obviously incorrect. This is probably caused by the errors involved in the measured intensity ratios of weak lines. In fact, there are some effects of T_ϵ fluctuation that may be considerably greater than that given by photoionization models or simple diagnostics (Peimbert et al. 1995). Peimbert (1967) gave a method for calculating the mean square fluctuation of T_ϵ throughout the radiating layers of a gaseous nebula, and an example of its application is found in Zuckerman & Aller (1986).

The problem of density diagnostics is unfortunately messy, as they may be strongly affected by small errors in the line intensity ratios. We find $N_\epsilon \sim$3200 cm^{-3}, from [O II]3726/3727 and [Cl III]5518/5538, while the auroral to nebular line ratio of [O II] indicates high density $\geq$ 10 000 cm^{-3}. The latter seems inappropriate. The high-dispersion 1907/1909 flux ratio from the *IUE* SWP 08175 yields an electron density of log N_ϵ = 3.7±0.1 or N_ϵ = 5000±1000 cm^{-3}. The [S III] result appears to also be in error, so we did not include this result in Fig. 2. A small observational error in some critical spectral lines can produce a large scatter in diagnostics, e.g. for ~10% errors in [O III] and [Ar III] lines, $\Delta T \sim \pm$1500K; and for ~15% in [Cl III], Δ log$N_\epsilon \sim \pm$0.3. So far, we have discussed diagnostics involving equivalent p^2 and p^4 electrons. With the forbidden lines involving the p^3 electrons, one can also obtain diagnostics for both density and temperature at the same time (see Keenan et al. 1999; 1997; 1996). (1) [O II]: λ3729/λ3726 vs. λ7320/(λ3726 + λ3729) gives (17 000 K, 5000 cm^{-3}), while λ3729/λ3726 vs. λ7330/(λ3726 + λ3729) gives (20 000 K, 5300 cm^{-3}). Similarly, (2) [Ar IV]: λ4711/λ4740 vs. λ7238/(λ4711 + λ4740) gives (8000 K, 3300 cm^{-3}), while λ4711/λ4740 vs. λ7263/(λ4711 + λ4740) gives (12 500 K, 5000 cm^{-3}); (3) [S II]: λ6717/λ6730 vs. λ4068/(λ6717 + λ6730) gives (15 000 K, 6200 cm^{-3}), while λ6717/λ6730 vs. λ4076/(λ6717 + λ6730) gives (20 000 K, 6300 cm^{-3}). The recent work of Keenan et al. involving p^3 electrons indicated excessive electron temperatures, though. The temperature information does not seem to be useful, while the density information appears to be correct. Thus, we adopt N_ϵ = 5000 cm^{-3} as a representative or average value for the whole nebula, which is also close to that found from the *IUE* 1907/1909 diagnostic ratio. A slightly higher density may be more appropriate, though. With equivalent d-electrons, there is also a diagnostic possibility. For example, Keenan et al. (2001) recently presented a new method to find a density from [Fe III] λ4658 vs. λ5011 or λ4986 (and from [Fe VII] lines as well). Unfortunately, in IC 5217, only [Fe III] 4658 has been measured, so we could not find the density information using the [Fe III] or [Fe VII] diagnostics.

3.2. Ionic Concentrations

With the appropriate electron temperature, T$_\epsilon$, and electron density, N_ϵ, we are now able to obtain the ionic concentrations by well-known formulae (see e.g. Aller 1984) updated using the most recent and reliable values of the atomic constants. Table 8 presents the ionic concentration calculated from the interstellar extinction corrected intensities, i.e. the near-UV ITS, UV region *IUE* and optical HES data listed in Tables 3, 4 and 6. Consecutive columns present the ion involved, its wavelength, intensity, and the values of N(ion)/N(H$^+$). For the electron temperature and density, we do not introduce a refinement of T$_\epsilon$ fluctuations, e.g. by making use of model predictions or diagnostics, but we apply the representative electron temperature and density, i.e. N_ϵ = 5000 cm^{-3} and T$_\epsilon$ = 10 700 K, adopted based on the argument made in Section 3.1.

In deriving He$^+$ abundances, we corrected for collisionally excited contributions. The HES λ4471 result disagrees with the HES λ5876 and λ6678 result. Comparison of the HES He I lines with the ITS He I lines (AC79; see Table 10) suggests that the HES λ4471 intensity may be in error. Our calculation shows the ITS λ4471 intensity gives He/H = 8.33(-2) [X(-Y) implies X ×

10^{-Y}, hereafter], in good agreement with the result from the other HES lines. Thus, we ignored the HES λ4471 result. The He II lines are relatively strong in this object, but they do not show a strong concentration in this ionization stage.

For the lines of carbon, nitrogen and silicon, we rely on our *IUE* measurements. As usual, ionic concentrations of C^{++} and C^{3+} are derived from the UV lines regarded as collisionally excited. Note that the O^{++} ionic concentration obtained from O III] 1661/66 approximately matches that from the optical [O III] lines. Virtually all of the O ions are accounted for by (O^{+}, O^{++}); likewise (Ne^{++}, Ne^{3+}) account for the neon ions. For sulfur, only two ionic concentrations (S^{+}, S^{++}) are found, but there is also a significant contribution from S^{3+}, which could not be derived here (see Section 5). We are also able to find the ionic concentration for other rare elements. Argon is mostly represented by Ar^{++} and Ar^{3+} with a weak contribution from Ar^{4+}. Sodium, potassium and silicon are represented by single ions, [Na IV] [K IV] and [Si III]. For chlorine, two ionic concentrations, Cl^{++} and Cl^{3+}, are available.

4. Theoretical Models

To construct a theoretical model, one must assume a distance to the PN along with certain properties of the CSPN. Distances found in the literatures show a large scatter, from 1.08 to 4.65 kpc (see Acker et al. 1992). We adopt a value close to the mean of these estimates and the relatively recent determination by Van de Steene & Zijlstra (1994; 2.66 and 2.23 kpc), i.e. 2.5 kpc. Our model investigation seems to be in favor of larger distances (see Section 6), though. The CSPN is classified between O and WR: in the Acker et al. Catalog of Galactic PNs (1992), the stellar type is listed as 'WNb?' which is highly unlikely for IC 5217. It has many C lines and should be WC. Köppen & Tarafdar (1978) derived the temperatures of CSPN, i.e. 54 000 K from [O^{++}/O^{+} ratio], 55 000 K from [λ5007/λ3727+λ3729 ratio], 86 000 K from [He(4471)/Hβ ratio], etc., showing a large scatter, and there appears to be no simple way of knowing the most appropriate one from such different indications. However, in our model investigation, a temperature for the CSPN can be relatively easily determined. We directly apply theoretical model atmospheres of some selected T_{eff} to photo-ionization modeling until the model predicts a correct level of nebular excitation (the energy-balance method and the Zanstra method). A number of preliminary trials with various non-LTE atmospheres from Hubeny's (1988) show that the CSPN must be in the range $T_{eff} \simeq$ 90 000 - 100 000 K.

Details of parameters adopted in our model are given in Table 9. The CSPN energy distribution used in the model is that of $T_{eff} = 92\,000$ K and log g = 5.5, with He/H = 0.085 and a nebular heavy element distribution in the central star. The nebular shell is assumed to be homogeneous with $N_{\rm H} = 5000$ cm^{-3}. No filling factor is introduced in the shell gas. We assume a central star radius of $R_* = 0.16 R_\odot$ and, as a result, $L_* = 1600\ L_\odot$. A small amount for the dust to gas ratio, $M_{dust}/M_{gas} = 0.005$, is assumed. For a distance of 2500 pc, the model reproduces the PN size and the absolute Hβ flux, within the observational errors. The outer boundary of the shell is material bounded with angular radius $\sim$ 3.9 arcsec. The observed absolute Hβ flux is F(Hβ) = 6.76($-$12) ergs cm^{-2} s^{-1}; and the absolute intrinsic flux is F_{corr}(Hβ) = 2.34 - 3.39($-$11) for C = 0.54 - 0.7, while the model predicts 3.18(-11) ergs cm^{-2} s^{-1} (see Tables 1 and 9). The observed visual magnitude is m_v = 15.5, and accordingly the intrinsic visual magnitude m_{v_o} = 14.4 using E_{B-V} = 0.37 (corresponding total extinction A_v here taken as 3.1E_{B-V}). The predicted intrinsic visual and blue magnitudes are m_v = 15.2 and m_b = 13.4, respectively.

Table 10 compares the observed and predicted intensities. The ITS and the HES + *IUE* data, are given in columns (3) and (4), respectively, while column (5) lists the predicted intensities from the model. All of the values are on the scale of I(Hβ) = 100. For most ions, a fairly reasonable agreement between the observed and predicted intensities is achieved, but in some cases, especially [S II] and [Ar IV], we find a glaringly large discordance. The agreement for He I is good, but the prediction for He II is close to the HES observation. The predictions for C seem fine except for the recombination C II λ4267 line. Predictions for the ions of N, O, Ne, and Cl seem generally successful. As noted in our previous investigations (see e.g. Hyung & Aller 1996), observed [S II] line intensities are stronger than predicted. Possibly the [S II] radiation is emitted in neutral region strata, or in an interface between the H I and H II domains: a shock heating involving geometrical complexity may also cause such a strong [S II] emission. The prediction for [S III] does not show any satisfactory result, either. Three rare elements are all represented by single ionization stages: sodium is represented by [Na IV], silicon by Si III], and potassium by [K IV]. Hence, agreement for these ions can be assured, and the abundances of these elements can be found by the model. For example, the [K IV] 6102 line (I = 0.20) is fitted by N(Ca)/N(H) = 5.0(-8), etc.

For the electron temperatures of [O II], [O III], and [O IV], the model predicts T_ϵ = 10 400 K, 10 600 K, and 11 900 K, respectively, which are close to the diagnostic indications by [N II], [O III], and [Ar III] (see Fig. 2). For other ions, our model predicts lower temperatures, i.e. $T_\epsilon \sim$ 10 300 K ([N II]) and 10 400 K ([Ar III]). Our model investigation implies that the CSPN temperatures derived by Köppen & Tarafdar (1978) would give very low gaseous temperatures and excitations. The photoionization model with the higher CSPN T_{eff} = 95 000 - 100 000 K, on the other hand, would predict relatively higher electron temperatures, T_ϵ = 12 000 - 13 500 K for the [O III] zone. The appropriate CSPN temperature of IC 5217 is likely to be around T_{eff} = 92 000 - 95 000 K.

5. Abundance Determinations

To determine the abundances in IC 5217, we implemented two methods: 1) using Ionization Correction Factors (ICFs) coupled with the derivation of ionic concentrations, and 2) using photoionization models. The latter predicts individual line intensities with the model described in Section 4, i.e. we modify the model parameters until a good fit is obtained, and we then adopt the model abundance; while the former uses the fractional ionic concentration in Section 3.2, and the correct ICFs for unobserved ionic stages predicted by the model.

The abundance of individual elements is given in Table 11. The 2nd column of this table lists the $\Sigma N(\text{ion})/N(\text{H}^+)$ and the 3rd column the ICF obtained from the theoretical model. The 4th column gives the final abundance N(ICF) obtained by applying the ICFs derived from the model. The 5th column gives the model abundances, N(model); the 6th column gives the logarithmic difference, i.e. $\Delta = \log N(\text{ICF}) - \log N(\text{Model})$; and larger discrepancies ($|\Delta| > 0.10$) are indicated for Ne, S, Ar, & Na. The 7th column gives the recommended abundance for IC 5217, while the 8th column lists the previous estimation by AC79. The last two columns list the 'average' PN abundance found by Aller and Czyzak (1983, hereafter AC83), and by Kingsburgh and Barlow (1984, hereafter KB), and the solar abundance by Grevesse and Noels (1993), respectively.

In general the ICF method gives results in good accord with the current model, but our determination shows a deviation from the AC79 result. The present abundance determination seems fairly reliable except for S and Ar. We believe our derivations are substantially improved over those by Aller & Czyzak (1979) and French (1981, 1983): their observations were carried out with a low to mid dispersion ITS, and only a limited number of lines were secured. The main purpose of the studies by French was to find the argon abundance from a spectrum obtained with the Lick Observatory 24 inch telescope. He found He/H ~ 0.117 (French 1981); ~0.1 (French 1983); and 0.1 (AC79), while our investigations suggest a very low value, i.e. He/H ~ 0.086, below the 'average' PN abundance and the solar value. We adopted the abundance of IC 5217 from the values close to the 'semi-traditional' determination, i.e. by the ICF-method rather than by modelling. Two obvious limitations may be pointed out in the modelling: 1) structural uncertainties, and 2) omission of the treatment of shocks in the prediction.

Determination of carbon abundance is always a difficult task, because of the absence of strong carbon emission lines in the optical region: derivation of the carbon abundance from the available weak optical permitted carbon lines, e.g. C II 4267, assuming that they are arising from recombination, used to give higher values by at least a factor of two, and then up to one order of magnitude, compared with those derived from the collisionally excited lines. We found C/H ~ 2.9(-4), based on the *IUE* data. Since the abundance derived here is for a gas phase, some carbon may be tied up in grains. Our derived C/H value is lower than the AC79 value by a factor of two. Apparently, carbon seems depleted, relative to the Sun or the average PN.

Contrary to the helium and carbon cases, we found the opposite result in nitrogen. Our derivation gives a value twice as large as the AC79 result, thus exceeding the average PN or the Sun. Oxygen is the case where our and AC79's results are in good accord within the observational errors, O/H ~ 4.5(-4) vs. 3.7(-4), which is close to the average PN, but less abundant than the Sun. We found a similar trend for Ne and Ar. Both Ne and Ar abundances appear close to the average PN value. The Ar abundance is fairly uncertain, though. The ICF method and the model both produce a chlorine abundance of 1.2(-7), which is only half of the AC79 value. Chlorine appears to be slightly less abundant than the average PN, but much lower than the Sun.

As mentioned in Section 5, the model could not fit the line intensities in both [S II] and [S III] lines. Thus, we must rely on the ICF method for sulfur abundance derivation. With an ICF of 4.12 for the unobserved stages of sulfur, i.e. S^{3+}, we found $S/H \simeq 3.88(-6)$. This value is only 1/2 of the model. AC79 derived an even higher value, 1.70(-5), though. If we adopt the S/H from a value close to an average of the ICF method and the model, sulfur may be close to or marginally lower than the average PN value. Roche & Aitken (1986) observed the infrared spectra of [S IV] 10.5μm (and [Ar III] 8.99μm) with UKIRT, but the used spectrometer aperture was smaller than the source. Thus, we could not use their measurement. They derived a relatively smaller concentration of 25% for the S^{3+} stage, assuming the relative sulfur abundance, $S/H \sim 1.0(-5)$ [probably quoted from AC79]. In contrast, our model calculation shows a high ionic concentration, i.e. 68% in the triple ionic stage.

Note that models do not take account of T_ϵ fluctuations such as would be produced by shock waves; hence the fluctuations found by models are smaller than those indicated by the Peimbert corrections. If we apply Peimbert T_ϵ fluctuation method in finding the abundances, we expect an abundance increase for C, N, and O, e.g. 10 - 20 % for $t^2 = 0.02$ (see Zuckerman & Aller 1986).

6. Conclusion

As discussed in Sec. 3.1, the most reliable electron temperatures may be determined from the diagnostic lines involving p^2 and p^4 electrons. For the electron density, one must also refer to the recent work by Keenan et al. involving p^3 electrons. Although IC 5217 is known as a mid-excitation PN with T_{eff} of about 50 000 - 60 000 K from previous investigations, our HES data analysis indicates the possibility of relatively high excitation. The [O III], [Ar III], [N II] and [Cl IV] diagnostics suggest a relatively high excitation. The model prediction seems to confirm this trend: the nebular electron temperatures are relatively higher, i.e. $T_\epsilon \leq 10\,700$ K and the CSPN temperature must be around $T_{eff} = 92\,000$ K, or slightly higher, to reproduce these electron temperatures.

Note that our study suggests lower He/H and C/H ratios in IC 5217, contrary to the previous results by AC79 or French (1983). However, we found no evidence of metal deficiency in other elements. S and Ar abundance determination is problematic. Although S, Si, and Na abundances involve a large ICF, only S appears to be serious disagreement. The prediction for sulfur lines shows a conspicuously large discordance, which may be caused by shock excitation in the emission. Ar seems always to be a problem (see e.g. Hyung et al. 2000). We also found difficulty in fitting argon lines. Thus, Ar and S abundances are poorly determined. Sulfur is very hard to handle because [S II] could all be produced in neutral H zone, so it is very hard to get the S/H ratio. If we adopted the smaller extinction coefficient, C, for the optical observations, the S^{++} abundance calculated from the intensities of the near-IR [S III] lines would increase, and the total sulfur abundance would also go up, improving agreement with the model, with AC79, and with "average" PN abundances.

Our assumed model geometry is a spherically symmetric shell. IC 5217 is an elongated PN with an e/p ratio of 4 or above: the radii of the bright elongated core of IC 5217 are $\sim 1'' \times 4''$ (see Balick 1987). Its structural evolution or shaping history may be explained by propagation of a wind-driven shock through a cylindrically symmetric red giant envelope. The shell ejected by the red giant had to be thinner in the polar than in the equatorial regions. This wind impinges on the quasi-toroidal envelope ejected by the red giant during its slow wind evolution on the asymptotic giant branch. There is no hint of any rotation. Since it is only partly radiation bounded (Icke et al. 1987), it would be better if it is analyzed via a composite model. In our previous modelling studies for a number of objects such as IC 2165 (Hyung 1994) and Hb 12 (Hyung & Aller 1996), we constructed a composite model with a density contrast between the equatorial and polar shells. We did not try such a refinement here, since it did not seem to improve the predictions much. With the availability of high spatial resolution spectral data through, e.g. Keck/HIRES, or Subaru/HDS, it would be worth constructing such a sophisticated model, in which one must also include a shock excitation mechanism to explain the [S II] emission lines.

If the assumed distance to PN IC 5217 is correct, the employed CSPN temperature (and surface gravity) and luminosity should give us a CSPN mass. Taking L($\star$) and T($\star$) at their face values (see Table 9), and utilizing Schönberner's (1983) evolutionary tracks, we derive a CSPN of about 0.55 $M_\odot$. An age of about 150 000 years, evolved from an AGB progenitor of about 0.8 solar mass, is implied, which is longer than the PN life time. If we adjust the distance to a large value, e.g. 5000 pc, then we expect a CSPN of 0.565 $M_\odot$ evolved from a one solar mass and 9000 year old progenitor. This simple analysis suggests that the true distance may be larger than the currently adopted one. In any case, the central star must have evolved from one solar mass, or a slightly less massive star, $\sim$0.9$M_\odot$, and the progenitor may have been an O-rich star (O/C ratio greater than 1). Nitrogen abundance is relatively high, compared with the average PN or the Sun: this may be due to the deep-mixing and dredge-up of N which may have formed from either O or C burning during the progenitor life time (see e.g. Briley et al. 1991; Sneden et al. 1994).

We are grateful to Dr. Karen Kwitter for a careful review and various helpful comments. We express our gratitude to the technical staff of Lick Observatory, who helped us secure these data. We are also grateful to Lauren Likkel whose weak line measurements made as a byproduct of a study of Bowen fluorescent emissions in a number of PN (LA86) proved very valuable. This research was supported by the grant KRF No. 2000-015-DP0445. S.H. is thankful to the staff of Supercomputing Center/KORDIC for permission to use the HPC320 supercomputer.

REFERENCES

Acker, A., Ochsenbein, F., Stenholm, B., Tylenda, R., Marcout, J., & Schohn, C., 1992, Strasbourg -ESO Catalogue of Galactic Planetary Nebulae, Garchung bei Munchen, European Southern Observatory

Aller, L. H., 1984, Physics of Thermal Gaseous Nebulae, (Dordrecht: Reidel Publisher)

Aller, L. H.. & Czyzak, S. J. 1979, Ap&SS, 1979, 62, 397 (AC79)

Aller, L. H., & Liller W., 1968, in Middlehurst B.M. and Aller, L.H., eds, Nebulae and Interstellar Matter, University of Chicago Press, Chicago, ch. 9, p498

Balick, B. 1987, AJ, 94, 671

Briley, M. M., Hesser, J. E., Bell, R. A. 1991, ApJ, 373, 482

Feklistova T., Kholtygin A.F. 1996, A New Atomic Line Catalogue for Planetary Nebulae, in private communication

French, H. B. 1983, ApJ, 273, 214

French, H. B. 1981, ApJ, 246, 434

Grevesse, N., Noels, A. 1993, in Origin and Evolution of Elements, ed. Prantzos, N., VangioniFlam, E. Casse, M. (Cambridge Univ. Press, Cambridge, U.K.), 15

Hyung, S. 1994, ApJS, 90, 119

Hyung, S., Aller, L. H. 1996, MNRAS, 278, 551

Hyung, S., Aller, L. H., Feibelman, W. A., Lee, W.-B., & de Koter, A. 2000, MNRAS, 318, 77

Icke, V., Preston, H. L., & Balick, B. 1987, ApJ, 97, 462

Kastner, S. O., & Bhatia, A. K. 1984, ApJ, 287, 945

Keenan, F. P., Aller, L. H., Bell, K. L., Crawford, F. L., Feibelman, W. A., Hyung, S., McKenna, F. C., & McLaughlin, B. M. 1999, MNRAS, 304, 27

Keenan, F. P., Aller, L. H., Bell, K. L., Hyung, S., McKenna, F. C., & Ramsbottom, C. A. 1996, MNRAS, 281, 1073

Keenan, F. P., Aller, L. H., Ryans, R. S. I., & Hyung, S. 2001, Proc. Natl. Acad Sci. USA, submitted

Keenan, F. P., McKenna, F. C., Bell, K. L., Ramsbottom, C. A., Wickstead, A. W., Aller, L. H., & Hyung, S. 1997, ApJ, 487, 457

Köppen, J., & Tarafdar, S. P., 1978, A&A, 69, 363

Likkel, L., & Aller, L. H. 1986, ApJ, 301, 825 (LA86)

Marionni, P. A., Harrington, J. P. 1980, The Universe at ultraviolet wavelengths, ed. R. D. Chapman, NASA CP-2171, 633

Moore, C. E. 1993, in J. W. Gallangher, ed. Tables of Spectra of H, C, N, and O, atoms and ions, CRC press, London

Moore, C. E. 1974, A Multiplet Table of Astrophys. Interest, National Bureau of Standards, No.40

Peimbert, M. 1967, ApJ, 156, 825

Peimbert, M., Uuridiana, V., & Torres-Peimbert, S. 1995, RMx.A&A, 31, 147

Phillips, J. P., & Pottasch, S. R. 1984, A&A, 130, 91

Pottasch, S. R. 1987, in IAU Symposium No. 103, Planetary Nebula, ed. D. R. Flower (Dordrecht, Reidel Publ), p.391

Roche, P. F., & Aitken D. K. 1986, MNRAS, 221, 63

Sabbadin, F. 1986, A&AS, 64, 579

Schönberner, B. 1983, ApJ, 272, 708

Sneden, C., Preston, G. W., McWilliam, A., & Searle, L. 1994, ApJ, 431, 27

Van de Steene, G. C., & Zijlstra A. A. 1994, A&AS, 108, 485

Wyse, A. B., 1942, ApJ, 95, 356

Zuckerman, B., & Aller, L.H. 1986, ApJ, 301, 772

This preprint was prepared with the AAS LaTeX macros v5.0.

Fig. 1.— The Ultraviolet Spectrum of IC 5217. Coadded plot from the three SWP 01923, 06257, 41909 and LWR 05429 [extinction correction applied with E(B-V) = 0.39]. Plot was smoothed by a three point running average.

Fig. 2.— Diagnostic diagram for IC 5217 — T_ϵ vs. log N_ϵ. Here [O II]2 refers to the transauroral to the nebular type transition. See Table 7 and text for additional diagnostics involving p^3 electrons.

Table 1. Some Basic Data for IC 5217, PN G 100.6 - 05.4.

Basic Data
$\alpha = 22^h 23^m 55\overset{s}{.}8$, $\delta = 50^\circ 58' 01''(2000)$,
Dimensions $\simeq 2\sim 6.6''$; N_ϵ: $\sim$5000 $\mathrm{cm^{-3}}$ (HAFL)
log F(Hβ) = -11.17 ± 0.01 [erg $\mathrm{cm^{-2}\ s^{-1}}$]
Excitation class: 6.0
Radial Velocity = -98.6 ± 0.4; 101.42 ± 038 (HAFL) km $\mathrm{s^{-1}}$
Expansion velocity = 17.5 & 25$\sim$28 km $\mathrm{s^{-1}}$ ([O III] & [N II]) [IPB87]
Central star: m_B 15.4, m_V 15.5, WC(WNb?)
T($\star$) = 92 000 $\sim$ 95 000 K (HAFL)

References. — HAFL: the present study; IPB87: Icke, Preston, & Balick (1987); Data not otherwise referenced are taken from Acker et al. (1992).

Table 2. IUE Observing Log for IC 5217.

Image number	Exposure (min.)	Date	Remarks
SWP 01923	40	1978 July 6	
SWP 08175	205	1980 Mar. 6	High-dispersion, noisy
SWP 06257	24	1979 Aug. 23	
SWP 41909	30	1991 June 24	
LWR 01785	40	1978 July 6	
LWR 05429	36	1979 Aug. 23	

Note. — An additional spectrum, SWP 07257, is listed in the archive but is a duplicate (tape replay) of SWP 06257.

Table 3. Emission Line Fluxes from SWP and LWR spectra.

λ(obs)	λ(rest)	Ion	k_λ[a]	Intensity	Flux[b]	Remarks
1163.38	1168.99	C IV	1.893	54	3.5	
1176.84	1175.50	C III	1.842	76	5.2	
1246.87	1238/40	N V	1.620	55	5.0	P Cyg emission, plus C III
1375.50	1371.29	O V]	1.345	3.2	0.4:	weak P Cyg emission
1432.89	1432.53	C I?	1.277	18	2.5	broad
1524.92	1526.71	Si II?	1.200	27	4.1	
1548.41	1548/50	C IV	1.184	58	9.1	
1562.48	1562.84	Si II?	1.175	7.0	1.1	
1576.88	1574.80	[Ne V]	1.166	24	3.8	blend C III 1575?
1622.52	1620.33	C III	1.143	9.2	1.5	
1640.79	1640.39	He II	1.136	61	10.1	
1664.16	1661/66	O III]	1.128	20	3.4	
1754.06	1746/70	N III]	1.120	15.7	2.6	SWP 06257 only
1815.32	1814.69	[Ne III]	1.140	6.7	1.1	
1890.01	1882/92	Si III]	1.204	7.3	1.1	
1907.83	1907/09	C III]	1.227	125	18.5	
2299.18	2297.57	C III	1.425	7.8	0.9:	
2322.58	2321/25	C II],[O III]	1.363	33	4.1	
2350.57	2353.24	[Ne IV]?	1.290	6.6	0.9:	
2398.78	2405.10	C IV	1.172	7.6	1.2	
2424.48	2422/24	[Ne IV]	1.115	12	2.1	
2471.88	2470.33	[O II]	1.022	8.4	1.6	
2518.91	2525/28	C IV	0.943	4.3	0.9	blend with He II 2511
2832.80	2836.00	C II	0.622	4.2	1.3	
2942.57	2941.65	O V?	0.551	3.2	1.1	
3021.17	3024.36	O III	0.508	2.2	0.8:	
3045.41	3047.13	O III	0.495	4.9	1.8	
3131.41	3132.90	O III	0.455	19	7.3	
3193.44	3187.74	He I	0.428	6.7	2.7:	

[a] the extinction parameter according to Seaton (1979)

[b] Measurements in the 1100 – 2000Å range are done from the 3 coadded spectra (SWP 01923, 06257, 41909), while in the 2000 – 3200Å range from LWR 05429.

Note. — The UV fluxes in col. (4) line intensities are in units of 10^{-13} ergs cm^{-2} s^{-1} and intensities are in Col. (5) are given based on the scale of I(Hβ) = 100 and the interstellar extinction corrections are done assuming $C = 0.54$ [or E(B-V)=0.39]. : means estimated errors are large, ±40%, others ±15%.

Table 4. Image Tube Scanner Observation of IC 5217.

λ(obs)	Ion	k_λ	Intensity	Flux	Remarks
3132.9	O III	0.454	19.7	11.2	B
3187.7	He I	0.431	3.11	1.82	
3303.2	He II	0.424	3.58	2.11	
3241.7	Na IV	0.409	0.79	0.47	
3299.4	O III	0.387	1.16	0.72	B
3312.3	O III	0.383	2.11	1.31	B
3340.8	O III	0.372	3.53	2.22	B
3362.2	Na IV	0.365	0.37	0.24	
3403.5	O IV	0.351	0.57	0.37	
3415.2	O III	0.347	0.54	0.35	B
3428.7	O III	0.334	1.41	0.92	B
3444.7	O III	0.338	7.33	4.82	B
3512.5	He I	0.317	0.40	0.27	
3552.0	He I	0.304	0.35	0.24	
3554.4	He I	0.305	0.36	0.25	
3587.3	He I	0.295	0.32	0.22	
3613.6	He I	0.288	0.25	0.18	
3634.3	He I	0.282	0.72	0.51	
3678.2	H I	0.270	0.29	0.21	
3682.1	H I	0.269	0.30	0.21	
3686.1	H I	0.268	0.50	0.36	

Note. — Measurements by Likkel from data secured at Lick observatory and B denotes a line of the Bowen fluorescent mechanism (Likkel & Aller 1986, LA86). Flux and intensity are on the scale of F(Hβ) = 100 and I(Hβ) = 100 (We applied an extinction correction with $C = 0.54$ adopted from the IUE one).

Table 5. Observing Log for Ground-based Observations

Set-up	Exposure (min)	Obs. Date (UT)
125 (800)	90	October 1, 1991
125 (800)	10	October 1, 1991
127 (800)	80	September 30, 1991
127 (800)	10	September 30, 1991
127 (800)	1	September 30, 1991
123 (800)	60	October 1, 1991
121 (800)	50	September 30, 1991
– (2048)	75	July 1, 1995
– (2048)	120	August 10, 1997
– (2048)	10	August 10, 1997
– (2048)	5	August 11, 1997

Note. — See text and Hyung (1994) for an explanation of 6 different set-up numbers, 125, 127, etc... for the 800×800 CCD chip settings.

Table 6. Hamilton Echelle Spectrum of IC 5217.

λ(obs)	λ(rest)	Ion	Mult.	k_λ	Int(HES)	Flux(HES)	RMS
3707.25	3707.24	O III	(14)	0.271	1.098	0.71	
3712.02	3711.97	H I	H15	0.269	1.913	1.24	28%
	3721.94	H I	H14				
3721.67	3721.83	[S III]	(2F)	0.267	2.721	1.77	12%
3726.04	3726.03	[O II]	(1F)	0.266	12.73	8.30	1%
3728.77	3728.82	[O II]	(1F)	0.265	6.613	4.32	26%
3734.31	3734.37	H I	H13	0.263	2.718	1.78	24%
3750.23	3750.15	H I	H12	0.259	2.788	1.84	21%
3754.75	3754.67	O III	(2)	0.258	0.664	0.44	
3759.87	3759.81	O III	(2)	0.256	1.736	1.15	18%
	3771.08	N III	(4)				
3770.55	3770.63	H I	H11	0.254	3.958	2.63	
3797.85	3797.90	H I	H10	0.246	5.733	3.85	10%
3819.60	3819.61	He I	(22)	0.241	2.135	1.45	77%
3835.35	3835.39	H I	H9	0.236	7.668	5.24	22%
3868.75	3868.71	[Ne III]	(1F)	0.228	120.4	83.37	11%
	3889.05	H I	H8				
3888.83	3888.65	He I	(2)	0.223	23.23	16.22	20%
3964.72	3964.73	He I	(5)	0.204	0.796	0.57	12%
3967.43	3967.41	[Ne III]	(1F)	0.203	47.47	34.20	14%
3970.07	3970.07	H I	Hϵ	0.203	16.57	11.95	9%
4026.19	4026.36	He I	(18)	0.189	2.574	1.90	4%
4068.62	4068.60	[S II]	(1F)	0.180	1.492	1.12	3%
4072.30	4072.16	O II	(10)	0.179	0.400	0.30	
	4076.35	[S II]	(1F)				
4076.05	4075.86	O II	(10)	0.178	0.540	0.41	12%
4093.07	4092.94	O II	(10)	0.174	0.425	0.32	
4097.34	4097.31	N III	(1)	0.173	1.775	1.34	17%
4101.72	4101.76	H I	Hδ	0.172	29.49	22.78	8%
4103.38	4103.37	N III	(1)	0.172	0.987	0.75	15%
4120.79	4120.81	He I	(16)	0.168	0.448	0.34	32%
	4143.77	O II	(106)				
4143.67	4143.76	He I	(53)	0.163	0.382	0.29	32%

Table 6—Continued

λ(obs)	λ(rest)	Ion	Mult.	k_λ	Int(HES)	Flux(HES)	RMS
4199.92	4199.83	He II	(4-11)	0.152	0.319	0.25	9%
4267.15	4267.18	C II	(6)	0.141	0.342	0.27	12%
4338.67	4338.67	He II	(4-10)	0.129	0.388	0.31	17%
4340.44	4340.47	H I	Hγ	0.129	49.43	40.16	4%
4363.17	4363.21	[O III]	(2F)	0.124	12.20	10.00	9%
4387.92	4387.93	He I	(51)	0.117	0.574	0.48	
4471.48	4471.48	He I	(14)	0.095	5.962	5.12	7%
4541.57	4541.59	He II	(9)	0.077	0.432	0.38	13%
4634.12	4634.16	N III	(2)	0.054	0.608	0.56	12%
4640.60	4640.64	N III	(2)	0.053	1.242	1.14	9%
4641.80	4641.81	N III	(2)	0.053	0.263	0.24	10%
4647.30	4647.40	C III	(1)	0.051	0.259	0.24	23%
4649.09	4649.14	O II	(1)	0.051	0.365	0.34	
4650.59	4650.84	O II	(1)	0.050	0.300	0.28	
4658.08	4658.10	[Fe III]	(3F)	0.049	0.255	0.24	33%
4661.72	4661.63	O II	(1)	0.048	0.155	0.14	
4676.28	4676.23	O II	(1)	0.044	0.102	0.09	
4685.71	4685.68	He II	(3-4)	0.042	10.78	10.07	8%
4711.38	4711.34	[Ar IV]	(1F)	0.036	3.866	3.65	8%
4713.17	4713.14	He I	(12)	0.036	0.624	0.59	5%
4740.20	4740.20	[Ar IV]	(1F)	0.029	4.361	4.16	17%
4859.29	4859.32	He II	(4-8)	0.000	0.613	0.61	24%
4861.29	4861.33	H I	Hβ	0.000	100.0	100.0	6%
4921.92	4921.93	He I	(48)	-0.015	1.303	1.33	26%
4931.27	4931.30	[O III]	(1F)	-0.017	0.173	0.18	26%
4956.07	4955.78	O II?	?	-0.022	0.087	0.09	
4959.02	4958.92	[O III]	(1F)	-0.023	594.0	616.6	5%
4969.29	4969.36	†		-0.026	0.303	0.32	23%
4996.26	4996.29	†		-0.032	0.473	0.50	12%
5006.85	5006.84	[O III]	(1F)	-0.034	1416.2	1496.2	11%
5015.68	5015.68	He I	(4)	-0.036	1.836	1.95	3%
5017.47	5017.48	†		-0.036	0.496	0.53	26%
5056.19	5056.35	Si II	(5)	-0.045	0.131	0.14	

Table 6—Continued

λ(obs)	λ(rest)	Ion	Mult.	k_λ	Int(HES)	Flux(HES)	RMS
5058.56	5058.40	†		-0.045	0.209	0.22	
5191.66	5191.80	[Ar III]	(3F)	-0.073	0.104	0.12	9%
5323.00	5323.30	[Cl IV]	(3F)	-0.100	0.056	0.07	
5345.96	5345.90	[Kr IV]	(1F)	-0.105	0.065	0.08	
5361.23	5361.64	Fe I?	?	-0.108	0.892	1.06	
	5412.00	[Fe III]	(1F)				
5411.53	5411.52	He II	(2)4-7	-0.118	0.890	1.08	21%
5462.76	5462.62	N II	(29)	-0.128	0.173	0.21	55%
5517.58	5517.71	[Cl III]	(1F)	-0.139	0.317	0.40	14%
5537.80	5537.88	[Cl III]	(1F)	-0.143	0.374	0.47	15%
5592.19	5592.37	O III	(5)	-0.155	0.068	0.09	
5679.89	5679.56	N II	(3)	-0.175	0.061	0.08	
5702.04	5702.43	Fe I?	?	-0.179	0.053	0.07	20%
5754.52	5754.64	[N II]	(3F)	-0.191	0.735	1.00	36%
5801.37	5801.51	C IV	(1)	-0.201	0.080	0.11	29%
5812.09	5811.98	C IV	(1)	-0.203	0.064	0.09	66%
5815.71	5815.97	†		-0.204	0.289	0.40	
5861.64	5861.11	Fe I?	?	-0.213	0.041	0.06	38%
5867.61	5867.82	He II,Si II	Pf29+	-0.214	0.036	0.05	
5875.63	5875.67	He I	(11)	-0.216	11.96	16.94	5%
5885.66	5885.90	†		-0.218	0.032	0.05	
6004.71	6004.72	He II	Pf22	-0.238	0.021	0.03	
6036.72	6036.78	He II	Pf21	-0.243	0.048	0.07	
6074.02	6074.19	He II	Pf20(8)	-0.249	0.031	0.05	
6083.76	6083.67	Fe I?	?	-0.251	0.072	0.11	15%
6101.75	6101.80	[K IV]	(1F)	-0.254	0.196	0.29	20%
6145.26	6145.42	Fe I?	?	-0.261	0.066	0.10	
6157.38	6157.73	Fe I?	?	-0.263	0.041	0.06	
6232.36	6232.6?	Fe I??	?	-0.274	1.633	2.54	
6233.78	6233.82	He II	Pf17(7)	-0.275	0.025	0.04	
6243.52	6243.13	Ar II?	(21)	-0.276	0.933	1.46	
6300.24	6300.30	[O I]	(1F)	-0.285	1.728	2.74	
6312.15	6312.10	[S III]	(3F)	-0.287	1.338	2.12	2%

Table 6—Continued

λ(obs)	λ(rest)	Ion	Mult.	k_λ	Int(HES)	Flux(HES)	RMS
6363.77	6363.78	[O I]	(1F)	-0.294	0.643	1.03	8%
6393.85	6393.62	[Mn V]?		-0.299	0.050	0.08	8%
6406.39	6406.38	He II	Pf15(7)	-0.301	0.065	0.11	18%
6435.10	6435.11	[Ar V]	(1F)	-0.305	0.072	0.12	43%
	6527.23	[N II]					
6527.09	6527.10	He II		-0.318	0.075	0.13	
6544.60	6544.50	†		-0.320	0.065	0.11	28%
6548.10	6548.03	[N II]	(1F)	-0.321	7.104	11.91	3%
6560.09	6560.10	He II	(4-6)	-0.322	1.298	2.18	9%
6562.78	6562.82	H I	Hα	-0.323	310.5	522.4	9%
6577.97	6578.03	C II	(2)	-0.325	0.068	0.11	1%
6583.40	6583.45	[N II]	(1F)	-0.326	24.72	41.78	15%
6601.63	6601.10	[Fe VII]	(1F)	-0.328	2.485	4.22	12%
6678.25	6678.15	He I	(46)	-0.338	2.852	4.92	21%
6683.17	6683.15	He II	Pf13(7)	-0.339	0.084	0.15	
6716.48	6716.47	[S II]	(2F)	-0.343	1.492	2.59	7%
6730.80	6730.85	[S II]	(2F)	-0.345	2.510	4.38	8%
6795.11	6795.00	[K IV]	(1F)	-0.352	0.056	0.10	
6891.28	6890.88	He II	Pf12(7)	-0.364	0.219	0.39	70%
7005.96	7005.70	[Ar V]	(1F)	-0.376	0.082	0.15	
7065.19	7065.28	He I	(10)	-0.383	4.677	8.67	5%
7135.72	7135.78	[Ar III]	(1F)	-0.391	9.367	17.58	4%
7170.80	7170.62	[Ar IV]	(2F)	-0.394	0.124	0.23	2%
7177.60	7177.50	He II	Pf11(6)	-0.395	0.115	0.22	5%
7237.30	7237.54	[Ar IV]	(2F)	-0.401	0.032	0.06	
7262.91	7262.96	[Ar IV]	(2F)	-0.404	0.098	0.19	
7281.41	7281.35	He I	(45)	-0.406	0.456	0.88	
7319.72	7319.40	[O II]	(2F)	-0.410	1.978	3.83	8%
7330.14	7320.90	[O II]	(2F)	-0.411	1.830	3.55	12%
7499.66	7499.84	He I	(1/8)	-0.428	0.067	0.13	
7530.35	7530.83	[Cl IV]	(1F)	-0.430	0.293	0.59	16%
7592.86	7592.74	He II	Pf10(6)	-0.436	0.113	0.23	4%
7751.06	7751.43	[Ar III]	(1F)	-0.451	1.863	3.85	10%

Table 6—Continued

λ(obs)	λ(rest)	Ion	Mult.	k_λ	Int(HES)	Flux(HES)	RMS
7816.09	7816.16	He I	(69)	-0.457	0.045	0.09	48%
8045.57	8046.27	[Cl IV]	(1F)	-0.477	0.680	1.47	14%
8115.06	8115.31	Ar I?	?	-0.482	0.418	0.91	
8196.67	8196.48	C III	(43)	-0.489	0.057	0.12	
8236.55	8236.78	He II	Pf9	-0.492	0.194	0.43	
8267.61	8267.94	H I	P34	-0.495	0.052	0.12	
8271.73	8271.93	H I	P33	-0.495	0.055	0.12	
8276.13	8276.31	H I**	P32	-0.495	0.063	0.14	
8281.02	8281.12	H I**	P31	-0.496	0.079	0.18	
8286.13	8286.43	H I	P30	-0.496	0.061	0.14	
8292.23	8292.31	H I	P29	-0.497	0.068	0.15	37%
8299.17	8298.84	H I	P28	-0.497	0.070	0.16	
8305.84	8306.12	H I**	P27	-0.498	0.047	0.10	
8313.92	8314.26	H I	P26	-0.498	0.074	0.16	
8323.04	8323.43	H I	P25	-0.499	0.068	0.15	
8333.74	8333.78	H I	P24	-0.500	0.067	0.15	
8344.28	8342.2?	He I?	(4/12)	-0.502	0.119	0.27	
8345.79	8345.55	H I	P23	-0.502	0.113	0.25	
	8359.66	He I					
8359.13	8359.01	H I	P22	-0.504	0.157	0.35	
8374.59	8374.48	H I	P21	-0.506	0.115	0.26	44%
8392.06	8392.40	H I	P20	-0.509	0.127	0.29	12%
8413.23	8413.32	H I	P19	-0.512	0.179	0.41	3%
8437.89	8437.96	H I	P18	-0.516	0.212	0.49	22%
8467.37	8467.26	H I	P17	-0.521	0.369	0.86	
8502.50	8502.49	H I	P16	-0.526	0.294	0.69	6%
8545.29	8545.38	H I	P15	-0.532	0.356	0.84	16%
8598.40	8598.39	H I	P14	-0.540	0.488	1.17	
8664.84	8665.02	H I	P13	-0.550	0.515	1.25	4%
8750.75	8750.48	H I	P12	-0.562	0.685	1.69	30%
8858.28	8859.1?	He II?	(6-22)	-0.577	0.058	0.15	
8862.82	8862.79	H I	P11	-0.578	1.375	3.49	
9014.70	9014.91	H I	P10	-0.599	1.062	2.79	

Table 6—Continued

λ(obs)	λ(rest)	Ion	Mult.	k_λ	Int(HES)	Flux(HES)	RMS
9068.88	9068.90	[S III]	(1F)	-0.606	9.615	25.53	6%
9229.00	9229.02	H I	P9	-0.612	1.550	4.16	3%
9344.81	9344.90	He II	Pf8(5-8)	-0.615	0.214	0.58	26%
9530.44	9531.00	[S III]	(1F)	-0.620	14.43	39.17	18%
9545.69	9545.97	H I**	P8	-0.620	1.927	5.24	8%
10028.33	10027.73	He I	(6/7)	-0.631	0.187	0.52	
10049.16	10049.38	H I	P7	-0.631	3.273	9.06	25%

[†] These unidentified lines are seen in other PNs, e.g. IC 4997 and NGC 7662.

[?,??] Unlikely or doubtful identification.

[**] Lines strongly affected by atmospheric absorption. Other lines not seriously affected by atmospheric absorption, are not marked.

Table 7. Diagnostic Line Ratios.

Ion	Lines	Ratio	Determines	Remarks
[N II]	$I(\lambda6548 + \lambda6583)/I(\lambda5755^{a})$	43.3	T_ϵ	
[O II]	$I(\lambda3726)$ / $I(\lambda3729)$	1.93	N_ϵ	[O II]1
[O II]	$I(\lambda3726 + \lambda3729)$ / $I(\lambda7319/20 + \lambda7329/30)$	5.08	N_ϵ,T_ϵ	[O II]2
[O III]	$I(\lambda4959 + \lambda5007)$ / $I(\lambda4363)$	166	T_ϵ	
[Cl III]^{a}	$I(\lambda5518)$ / $I(\lambda5538)$	.848	N_ϵ	
[Cl IV]	$I(\lambda7530 + \lambda8045)$ / $I(\lambda5323)$	17.4	T_ϵ	
[Ar III]	$I(\lambda7136 + \lambda7751)$ / $I(\lambda5191^{a})$	108	T_ϵ	
[S III]	$I(\lambda9069 + \lambda9531^{a})$/ $I(\lambda6312)$	18.0	T_ϵ	N/A ?
[S II]	$I(\lambda6717^{b})$/ $I(\lambda6731)$	.594	N_ϵ	N/A ?
[Ar IV]	$I(\lambda4711)$ / $I(\lambda4740)$	.886	N_ϵ	N/A ?

[a] relatively weak line or poor quality.

[b] $\lambda6717$ line measurement is always affected by the drip from a strong Hα in adjacent echelle order, so the actual error would be larger than the RMS % error, i.e. 6% in Table 6.

Note. — N/A ?: diagnostic informations are useless or not in a reasonable range (observational errors or poor measurements). For T_ϵ([S III]), the other $I(\lambda9069)/I(\lambda6312)$ ratio implies a temperature of about 15 000 K, close to T_ϵ([Cl IV]). However, IC 5217 is a medium excitation PN and thus these excessive values are perhaps in error.

Table 8. Fractional Ionic Concentration.

Ion	Wavelength	Inten.	$\frac{N(ion)}{N(H^+)}$	$\Sigma\frac{N(ion)}{N(H^+)}$
He I	6678	2.85	7.08(-2)	
	4471(HES)	5.96	1.19(-1)	
	4471(ITS)[a]	4.17	8.33(-1)	
	5876	11.96	7.85(-2)	
He II	4686	10.78	9.14(-3)	
	5412	0.89	5.55(-3)	8.59(-2)[b]
C III	1907/09	125.4	1.93(-4)	
C IV	1549/51	58.6	8.55(-5)	2.78(-4)
N II	6548/84,5755	32.56	4.07(-6)	
N III	1746–53	15.7	1.23(-4)	1.27(-4)
O I	6300/63	2.37	2.05(-6)	
O II	3727/29,7320/30	16.54	7.48(-6)	
O III	4957,5007,4363	2022.4	4.41(-4)	4.50(-4)
O III	1661/66	20.3	5.64(-4)[c]	
Ne III	3869/3967	167.8	8.08(-5)	
Ne IV	2422/24	12.4	1.65(-5)	9.73(-5)
S II	6717/31,4068	5.49	1.59(-7)	
S III	6312,9069,9552	25.38	7.83(-7)	9.42(-7)
Ar III	7135,7751,5192	11.33	6.54(-7)	
Ar IV	4711/40,7263/40,7172	8.48	7.16(-7)	
Ar V	6435,7006	0.154	1.60(-8)	1.37(-6)
Cl III	5517/37	0.691	4.02(-8)	
Cl IV	7530/8045,5323	1.03	5.77(-8)	9.79(-8)
Na IV	3242/3362	1.16	1.40(-6)	1.40(-6)

Table 8—Continued

Ion	Wavelength	Inten.	$\frac{N(ion)}{N(H^+)}$	$\Sigma\frac{N(ion)}{N(H^+)}$
K IV	6102	0.196	4.50(-8)	4.50(-8)
Si III	1882/92	7.3	2.40(-6)	2.40(-6)

[a] ITS measurement by Aller & Czyzak (1979).

[b] weighted by intensity.

[c] discarded because of its large scatter or uncertain intensity.

Note. — X(-Y) implies X × 10^{-Y}. Ionic concentrations are derived with N_ϵ = 5000 cm^{-3} and T_ϵ = 10 700 K. Atomic data used in the calculation are from many sources, e.g. from Keenan et al. (1996, 1997, 1999), from Aller (1984) or the compilation by Feklistova and Kholtygin (1996).

Table 9. Model Details for IC 5217.

Parameter	Model
R_{in}(pc)	0.035
R_{out}(pc)[a]	0.047 (3.9″)
N_H(cm^{-3})	5000
DISTANCE =	2500 pc
M_{dust}/M_{gas} =	0.005
F(Hβ)–obs[b] =	$2.34 \sim 3.39(-11)$ ergs cm^{-2} s^{-1}
F(Hβ)–prd =	$3.18(-11)$ ergs cm^{-2} s^{-1}
CSPN T($\star$)[c] =	92 000 K (log g = 5.5)
CSPN R($\star$) =	0.16 $R_\odot$ (L($\star$) = 1600 $L_\odot$)
T_ϵ([O II, III, IV])	10 400,10 600,11 900 K
Magnitude	V_{prd} = 15.2 & V_{obs} = 14.4[d]

[a] density bounded.

[b] extinction corrected with $C = 0.54 \sim 0.7$.

[c] Hubeny non-LTE model atmosphere. See text.

[d] corrected with E(B-V)=0.37.

Table 10. Comparison of Observed and Predicted Intensities for IC 5217.

El–ion	λ	ITS^a	I(HES-IUE)	I(Model)
He I	5876	12.3	11.96	11.97
	6678	3.63	2.85	3.14
	4471	4.17	5.96	4.21
He II	4686	14.1	10.77	8.14
	5412	0.98	0.89	0.66
	1640		[61]	56.4
C II	2325/28		...	8.8
	4267	0.22	0.34	0.17
C III	1907/09		[125.4]	108.6
C IV	1548/51		[58.6]	65.0
N II	6584	24.5	24.72	24.76
	6548	7.76	7.10	8.55
	5755	0.63	0.73	0.53
N III	1747-52		[15.7]	17.9
N IV	1483/86		...	7.84
O II	3726	17.4	12.73	12.67
	3729	7.9	6.61	5.68
	7321/2	...	1.98	0.99
	7332/3	...	1.83	0.79
O III	1660/66		[20.3]	17.1
	4363	11.5	12.20	12.33
	4959	417	594	491.8
	5007	1175	1416	1417
Ne III	3868	107	120.4	120.4
	3969	44.7	47.47	35.91
Ne IV	2422/25		[12.4]	3.36
	4725/27		...	0.02
S II	4068	1.90	1.49	0.07
	4076	0.70	0.54	0.02
	6717	1.28	1.49	0.10
	6731	2.57	2.51	0.18
S III	6312	1.44	1.34	0.34
	9069	...	9.62	5.93

Table 10—Continued

El–ion	λ	ITS[a]	I(HES-IUE)	I(Model)
	9531	...	14.43	14.43
Cl III	5518	0.39	0.32	0.35
	5538	0.51	0.37	0.50
Cl IV	7530	0.36	0.30	0.29
	8046	0.79	0.68	0.68
Ar III	5193	0.08	0.10	0.07
	7136	9.77	9.37	9.36
	7751	2.14	1.86	2.26
Ar IV	4711	4.68	3.87	7.60
	4740	4.37	4.36	9.29
	7238	0.25	0.03	0.15
	7263	0.07	0.10	0.17
	7171	?	0.12	0.20
Ar V	6435	...	0.07	0.09
	7005	...	0.08	0.19
Na IV	3242		[0.79]	0.83
	3362		[0.37]	0.36
K IV	6102	0.16	0.20	0.19
Si III	1883/92		[7.3]	6.3

[a] Aller & Czyzak (1979, AC79).

Note. — [I(HES-IUE)]: Intensities in bracket are the low resolution *IUE* and LA86 ITS data.

Table 11. Comparison of ICF and Model Abundances for IC 5217.

Elem.	$\Sigma \frac{N(ion)}{N(H^+)}$	ICF	N(ICF)	N(Model)	Δ	IC 5217	AC79	Mean[a]	SUN[b]
He I, II	8.59(-2) 9.80(-2)[c]	1.	8.59(-2)	8.60(-2)	–	8.6(-2)	0.1	0.11	0.1
C III, IV	2.78(-4)	1.04	2.90(-4)	2.90(-4)	0.00	2.9(-4)	5.63(-4)	6.48(-4)	3.55(-4)
N II, III	1.27(-4)	1.51	1.92(-4)	2.05(-4)	-0.03	2.0(-4)	1.06(-4)	1.40(-4)	9.33(-5)
O I, II, III	4.50(-4)	1.03	4.62(-4)	4.10(-4)	0.05	4.5(-4)	3.66(-4)	4.93(-4)	7.41(-4)
Ne III, IV	9.73(-5)	1.00	9.73(-5)	7.50(-5)	0.11	9.7(-5)	8.36(-5)	1.25(-4)	1.17(-4)
S II, III	9.42(-7)	4.12	3.88(-6)	1.00(-5)	-0.41	4.0(-6)	1.70(-5)	8.08(-6)	1.62(-5)
Ar III, IV, V	1.37(-6)	1.00	1.37(-6)	2.53(-6)	-0.27	2.0(-6)	2.25(-6)	2.42(-6)	3.98(-6)
Cl III, IV	9.79(-8)	1.18	1.15(-7)	1.18(-7)	-0.01	1.2(-7)	2.29(-7)	1.66(-7)	3.88(-7)
Na IV	1.40(-6)	13.5	1.88(-5)	1.50(-5)	0.10	1.5(-5)	···	···	2.06(-6)
K IV	4.50(-8)	1.12	5.04(-8)	5.00(-8)	0.00	5.0(-8)	3.26(-8)	···	1.35(-7)
Si III	2.40(-6)	2.77	6.65(-6)	5.50(-6)	0.08	6.0(-6)	···	···	3.55(-5)

[a] Average (or normal) abundances by Kingsburgh & Barlow (1994) and Aller & Czyzak (1983)

[b] Solar abundances by Grevesse and Noels (1993).

[c] With the HES λ4471 result included (see Table 8).

Note. — X1,X2(-Y) implies X1 × 10^{-Y}, X2 × 10^{-Y}. Δ: the logarithmic difference, i.e., $\log N$(ICF) $- \log N$(Model).

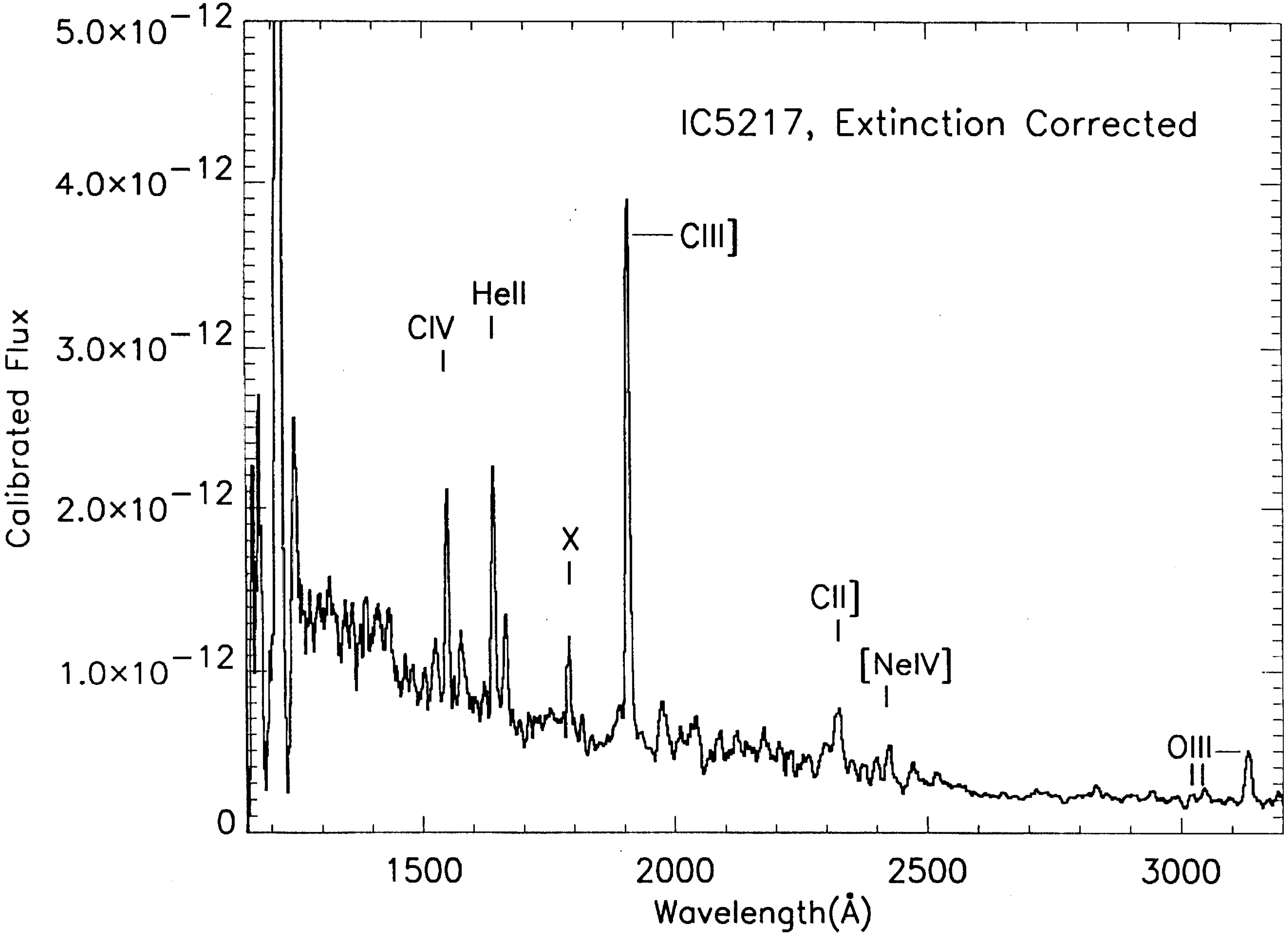
IC5217, Extinction Corrected
CIV
HeII
X
CIII]
CII]
[NeIV]
OIII
Calibrated Flux
5.0×10^{-12}
4.0×10^{-12}
3.0×10^{-12}
2.0×10^{-12}
1.0×10^{-12}
0
1500
2000
2500
3000
Wavelength(Å)

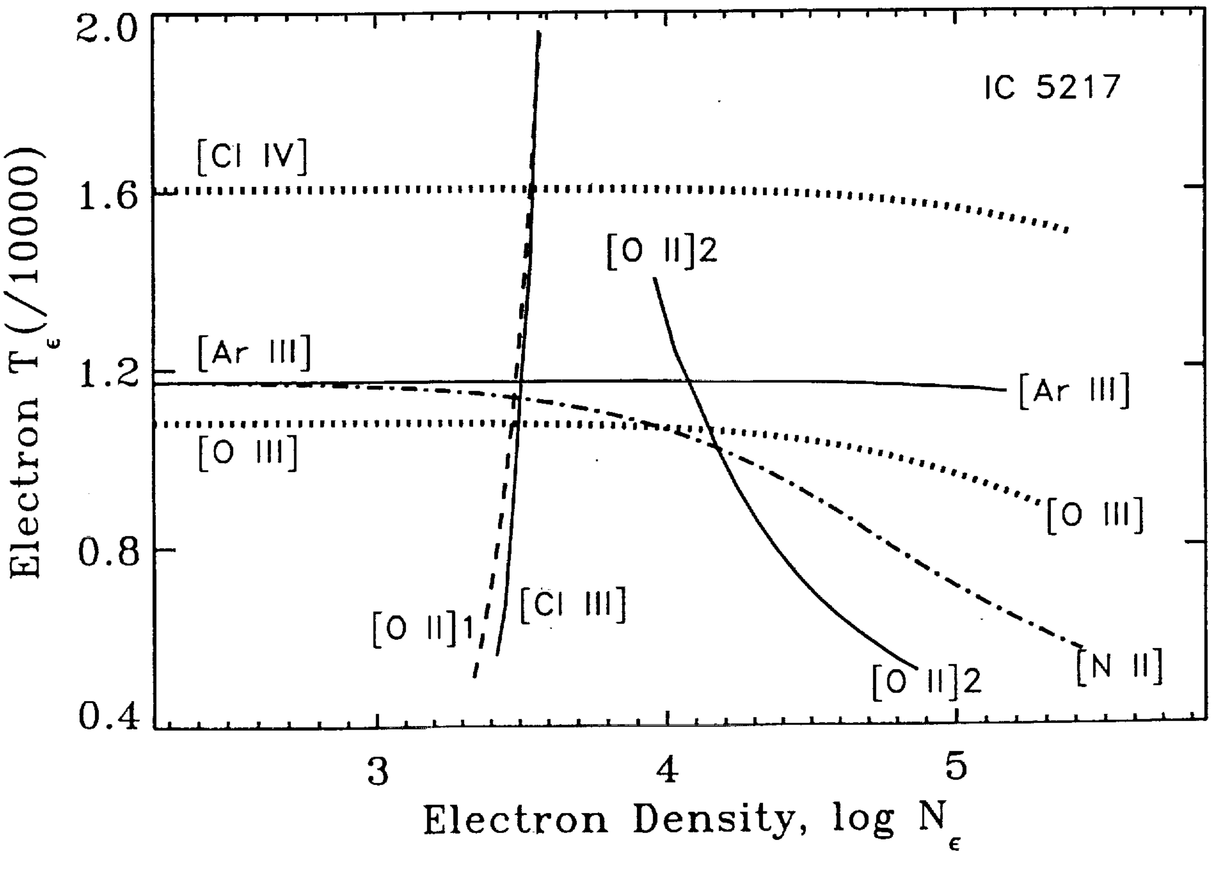

IC 5217
[Cl IV]
[Ar III]
[O III]
[O II]2
[Ar III]
[O III]
[O II]1
[Cl III]
[O II]2
[N II]
2.0
1.6
1.2
0.8
0.4
3
4
5
Electron T_ϵ(/10000)
Electron Density, log N_ϵ